Draft version May 18, 2017
Typeset using LaTeX **twocolumn** style in AASTeX61

A MULTI-TELESCOPE CAMPAIGN ON FRB 121102: IMPLICATIONS FOR THE FRB POPULATION

C. J. Law,[1] M. W. Abruzzo,[2] C. G. Bassa,[3] G. C. Bower,[4] S. Burke-Spolaor,[5,6,7] B. J. Butler,[5] T. Cantwell,[8] S. H. Carey,[9] S. Chatterjee,[10] J. M. Cordes,[10] P. Demorest,[5] J. Dowell,[11] R. Fender,[12] K. Grainge,[8] J. W. T. Hessels,[3,13] J. Hickish,[1,9] V. M. Kaspi,[14] T. J. W. Lazio,[15] M. A. McLaughlin,[6,7] D. Michilli,[3,13] K. Mooley,[12] Y. C. Perrott,[9] S. M. Ransom,[16] N. Razavi-Ghods,[9] M. Rupen,[17] A. Scaife,[8] P. Scott,[9] P. Scholz,[17] A. Seymour,[18,19] L. G. Spitler,[19] K. Stovall,[5,11] S. P. Tendulkar,[14] D. Titterington,[9] R. S. Wharton,[10] and P. K. G. Williams[20]

[1] *Department of Astronomy and Radio Astronomy Lab, University of California, Berkeley, CA 94720, USA*
[2] *Haverford College, 370 Lancaster Ave, Haverford, PA 19041, USA*
[3] *ASTRON, Netherlands Institute for Radio Astronomy, Postbus 2, 7990 AA, Dwingeloo, The Netherlands*
[4] *Academia Sinica Institute of Astronomy and Astrophysics, 645 N. A'ohoku Place, Hilo, HI 96720, USA*
[5] *National Radio Astronomy Observatory, Socorro, NM 87801, USA*
[6] *Department of Physics and Astronomy, West Virginia University, Morgantown, WV 26506, USA*
[7] *Center for Gravitational Waves and Cosmology, West Virginia University, Chestnut Ridge Research Building, Morgantown, WV 26505*
[8] *Jodrell Bank Centre for Astrophysics, Alan Turing Building, School of Physics & Astronomy ,The University of Manchester, Oxford Road, Manchester M13 9PL, UK*
[9] *Astrophysics Group, Cavendish Laboratory, 19 J. J. Thomson Avenue, Cambridge CB3 0HE, UK*
[10] *Cornell Center for Astrophysics and Planetary Science and Department of Astronomy, Cornell University, Ithaca, NY 14853, USA*
[11] *Department of Physics and Astronomy, University of New Mexico, Albuquerque, NM 87131, USA*
[12] *Centre for Astrophysical Surveys, University of Oxford, Denys Wilkinson Building, Keble Road, Oxford OX1 3RH, UK*
[13] *Anton Pannekoek Institute for Astronomy, University of Amsterdam, Science Park 904, 1098 XH Amsterdam, The Netherlands*
[14] *Department of Physics and McGill Space Institute, McGill University, 3600 University St., Montreal, QC H3A 2T8, Canada*
[15] *Jet Propulsion Laboratory, California Institute of Technology, Pasadena, CA 91109, USA*
[16] *National Radio Astronomy Observatory, Charlottesville, VA 22903, USA*
[17] *National Research Council of Canada, Herzberg Astronomy and Astrophysics, Dominion Radio Astrophysical Observatory, P.O. Box 248, Penticton, BC V2A 6J9, Canada*
[18] *Arecibo Observatory, HC3 Box 53995, Arecibo, PR 00612, USA*
[19] *Max-Planck-Institut für Radioastronomie, Auf dem Hügel 69, D-53121 Bonn, Germany*
[20] *Harvard-Smithsonian Center for Astrophysics, Cambridge, MA, USA*

ABSTRACT

We present results of the coordinated observing campaign that made the first subarcsecond localization of a Fast Radio Burst, FRB 121102. During this campaign, we made the first detection of an FRB burst by multiple telescopes: the VLA at 3 GHz and the Arecibo Observatory at 1.4 GHz. Of the nine bursts detected by the Very Large Array at 3 GHz, four had simultaneous observing coverage at other observatories. We use multi-observatory constraints and modeling of bursts seen only at 3 GHz to confirm earlier results showing that burst spectra are not well characterized by a power law. We find that burst spectra are characterized by a ~ 500 MHz envelope and apparent radio energy as high as 10^{40} erg. We measure significant changes in the apparent dispersion between bursts that can be attributed to frequency-dependent profiles or some other intrinsic burst structure that adds a random error to the estimate of DM by up to 1%. We use FRB 121102 as a prototype of the FRB class to estimate a volumetric birth rate of FRB sources $R_{\rm FRB} \approx 5 \times 10^{-5}/N_r$ Mpc^{-3} yr^{-1}, where N_r is the number of bursts per source over its lifetime. This rate is broadly consistent with models of FRBs from young pulsars or magnetars born in superluminous supernovae or long gamma-ray bursts, if the typical FRB repeats on the order of 10^3 times during its lifetime.

1. INTRODUCTION

Fast Radio Bursts (FRBs) were discovered ten years ago with the detection of a millisecond-duration radio transient with an anomalously high dispersion measure (Lorimer et al. 2007). The largest measured DMs imply that FRBs originate outside of our Galaxy, potentially at cosmological distances, and are orders of magnitude more luminous than pulses from Galactic pulsars (Thornton et al. 2013). There are now 21 FRBs publicly known [1] with dispersion measures (DMs) as high as 1600 pc cm^{-3} and intrinsic temporal widths of order milliseconds. Both their energetics and distance have inspired a wide variety of models and astrophysical applications (e.g., McQuinn 2014; Kulkarni et al. 2014; Fuller & Ott 2015; Connor et al. 2016b; Cordes & Wasserman 2016; Popov & Pshirkov 2016). However, that potential was limited by the lack of a definitive association of an FRB to an extragalactic host.

This paper is part of a series based on the first localization of an FRB and its unambiguous association to an extragalactic host (Chatterjee et al. 2017; Tendulkar et al. 2017; Marcote et al. 2017). FRB 121102, also known as the "repeating FRB", was discovered (Spitler et al. 2014) in data acquired in 2012 as part of the PALFA survey of the Arecibo Observatory (Cordes et al. 2006). In mid 2015, new Arecibo observations revealed a series of bursts at a similar DM and sky position that rules out cataclysmic models for this source (Spitler et al. 2016). The typical DM measured by early Arecibo observations was 559 pc cm^{-3} (Scholz et al. 2016), although somewhat higher values have been seen in more recent observations (560.5 pc cm^{-3}; Hessels et al., in prep).

Beginning in August of 2015 (MJD 57623), we made the first of nine detections of FRB 121102 with the Karl G. Jansky Very Large Array (VLA; Chatterjee et al. 2017) and localized it with a precision of $0.1''$. Deep optical observing with the Gemini Observatory associated the FRB with a host galaxy at $z = 0.193$ (Tendulkar et al. 2017) and the European VLBI Network detected four more bursts to localize the source with a precision of $0.01''$, four orders of magnitude better than any other FRB (precision of ~ 40 pc in linear distance; Marcote et al. 2017). The lookback and luminosity distances for FRB 121102 are 746 and 972 Mpc, respectively, assuming a concordance cosmology with parameters given by Planck Collaboration et al. (2016). If FRB 121102 is representative of all FRBs, then we should expect them to be useful as probes of the intergalactic medium and their host galaxies. Thus, the confirmation of a cosmological distance for FRB 121102 has begun to fulfil the promise implied by the first FRB detection.

Many new models for the origin of FRBs have been developed in response to the localization of FRB 121102 (Kashiyama & Murase 2017; Metzger et al. 2017; Zhang 2017; Dokuchaev & Eroshenko 2017; Beloborodov 2017; Thompson 2017). The association of FRB 121102 with a compact, persistent radio source is consistent with bursts coming from a young magnetar that powers a luminous pulsar wind nebula (Kashiyama & Murase 2017). At the same time, FRB 121102 is found in a low-metallicity dwarf galaxy (Tendulkar et al. 2017; Metzger et al. 2017), which was not predicted by origin models that scale with stellar mass or star formation (Nicholl et al. 2017). These galaxies are the preferred environment for long GRBs and Type-I superluminous supernovae (LGRB and SLSN-I, respectively), which have been suggested are signatures of the magnetar birth (Modjaz et al. 2008; Lunnan et al. 2014).

This paper presents an analysis of the spectral properties of VLA bursts implied by simultaneous observing at Arecibo, Effelsberg, the first station of the Long-Wavelength Array (LWA1; Ellingson et al. 2013), and the Arcminute Microkelvin Imager Large Array (AMI-LA; Zwart et al. 2008). This includes the first simultaneous detection of an FRB at two observatories, between the VLA and Arecibo. If we assume that FRB 121102 is representative of all FRBs, we can use it to constrain the physical processes at play in the overall FRB population. The repetition of FRB 121102 also has strong implications for calculations of their rate of occurrence (Connor et al. 2016a) and comparison to other classes of transient, such as superluminous supernovae (Tendulkar et al. 2017).

In Section 2, we describe the multi-telescope observing campaign and a refined analysis of the nine VLA bursts. Section 3 presents the first spectrum of an FRB simultaneously detected at multiple telescopes and confirm that burst spectra cannot be modeled with a single spectral index. We then model the dynamic spectra to characterize the burst spectra, energies, and dispersion properties. Section 4 discusses the properties of FRB 121102 bursts and its impact on inferences about the birth rate of FRB sources and strategies to find and/or localize new FRBs.

2. OBSERVATIONS

The data presented here were obtained from multiple programs and telescopes with a goal of interferometrically localizing FRB 121102 with the VLA. We coordinated observing between the VLA, Arecibo, Effelsberg,

[1] See `http://www.astronomy.swin.edu.au/pulsar/frbcat`.

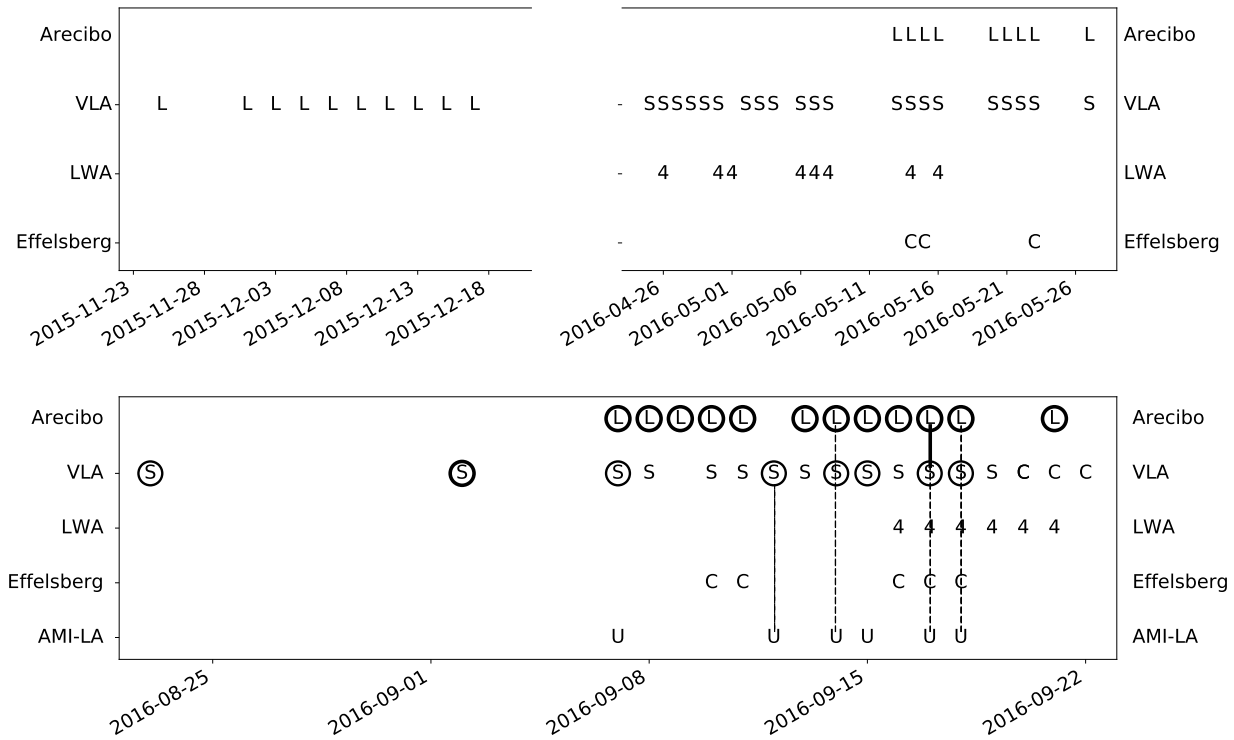

Figure 1. The top and bottom panels summarize the observations and detections of FRB 121102 in the 2015 and 2016 campaigns. Circles highlight observations that detected bursts from FRB 121102 with multiple burst detections indicated with a heavy line. The black dashed lines show the VLA burst detections with simultaneous coverage at other telescopes and the solid line shows the simultaneous burst detection. Circled observations with no line indicate bursts that did not have simultaneous observing coverage at the VLA. Days with observations are indicated with radio band designations 4, L, S, C, U referring to radio frequencies of 70 MHz, 1.4, 3, 4.5, and 15 GHz, respectively.

LWA1, and AMI-LA telescopes, as shown in Figure 1 and Table 1. Below, we summarize these observations, with a focus on those conducted simultaneously with VLA burst detections from FRB 121102.

Computational (Jupyter) notebooks to reproduce the transient detection, localization, and analysis presented here can be found at `https://github.com/caseyjlaw/FRB121102`. Time cut-out visibility data and calibration products are available at `https://doi.org/10.7910/DVN/TLDKXG`. Original VLA visibility data are available under NRAO program codes 16A-459 and 16A-496 and can be downloaded at `http://archive.nrao.edu`.

Table 1. Table of VLA Observations

MJD	Date/time (ymd/hms)	Duration (min)	Freq. (GHz)	Bursts
57351	2015-11-25/3:25:29	60	1.4	0
57357	2015-12-01/5:31:31	60	1.4	0
57359	2015-12-03/2:53:57	60	1.4	0
57361	2015-12-05/4:45:44	60	1.4	0
57363	2015-12-07/4:37:50	60	1.4	0
57365	2015-12-09/9:29:25	60	1.4	0
57367	2015-12-11/9:22:27	60	1.4	0
57369	2015-12-13/9:13:7	60	1.4	0
57371	2015-12-15/9:6:16	60	1.4	0
57373	2015-12-17/8:57:51	60	1.4	0
57503	2016-04-25/23:21:39	240	3	0
57504	2016-04-26/23:14:31	120	3	0
57505	2016-04-27/23:26:09	120	3	0
57506	2016-04-28/22:41:31	120	3	0
57507	2016-04-29/22:37:34	120	3	0
57508	2016-04-30/19:14:46	60	3	0
57510	2016-05-02/23:14:18	60	3	0

Table 1 continued

Table 1 *(continued)*

Table 1 continued

Table 1 *(continued)*

57511	2016-05-03/22:53:26	60	3	0
57514	2016-05-06/18:25:12	60	3	0
57515	2016-05-07/19:34:13	60	3	0
57516	2016-05-08/19:30:20	60	3	0
57521	2016-05-13/17:12:48	135	3	0
57522	2016-05-14/17:14:11	135	3	0
57523	2016-05-15/17:15:26	135	3	0
57524	2016-05-16/16:59:52	135	3	0
57528	2016-05-20/16:45:46	135	3	0
57529	2016-05-21/16:44:6	135	3	0
57530	2016-05-22/16:43:53	135	3	0
57531	2016-05-23/16:44:11	135	3	0
57535	2016-05-27/16:29:34	135	3	0
57623	2016-08-23/17:26:28	54	3	1
57633	2016-09-02/15:52:17	54	3	2
57638	2016-09-07/10:14:50	120	3	1
57639	2016-09-08/10:14:40	120	3	0
57641	2016-09-10/9:59:36	120	3	0
57642	2016-09-11/9:59:49	120	3	0
57643	2016-09-12/9:15:19	120	3	1[d]
57644	2016-09-13/9:23:59	120	3	0
57645	2016-09-14/9:20:23	120	3	1[a,d]
57646	2016-09-15/9:16:29	120	3	1
57647	2016-09-16/9:11:23	120	3	0
57648	2016-09-17/8:59:20	120	3	1[a,*,b,c,d]
57649	2016-09-18/8:59:27	120	3	1[a,b,c,d]
57650	2016-09-19/8:44:32	120	3	0
57651	2016-09-20/8:44:33	120	3	0
57651	2016-09-20/17:19:3	120	6	0
57652	2016-09-21/9:13:57	120	6	0
57653	2016-09-22/9:12:24	120	6	0

NOTE—Times are in UT. Frequency is the approximate center of the bandwidth.

[a] Arecibo coverage at 1.4 GHz.

[*] Arecibo detection at 1.4 GHz.

[b] Effelsberg coverage at 4.5 GHz.

[c] LWA1 coverage near 62 and 78 MHz.

[d] AMI-LA coverage at 15 GHz.

2.1. *VLA*

The FRB 121102 observing campaign started in November 2015 with a 10 hr campaign ($\sim$ 1 hr per session) observed at 1.4 GHz in the compact D configuration. In April through May 2016, we conducted a 40 hr campaign ($\sim$ 2 hr per session) at 3 GHz in the C and CnB configurations in coordination with Arecibo (Scholz et al. 2016). We concluded with a 40 hr, coordinated campaign ($\sim$ 2 hr per session) from August through September 2016 in the B configuration and during the move to the most extended A configuration. In the late-2016 campaign, the first 34 hours of VLA observations were made at 3 GHz, while the last 6 hours were observed at 6 GHz. These observing session times are inclusive of calibration and overhead, which typically amounts to 15% of the total observing time.

All VLA fast-sampled data were observed with 5 ms sampling, 256 channels, and dual-circular polarization (Law et al. 2015). The total bandwidths at L (1.4 GHz), S (3 GHz), and C (6 GHz) bands were 256, 1024, and 2048 MHz, respectively, corresponding to channel bandwidths of 1, 4, and 8 MHz. The dispersion smearing across a channel is $\sim$ 1.7, 0.7, and 0.2 ms in the same respective bands. The 3 GHz data were recorded data in eight spectral windows with 32 channels each and had sensitivity of 5 mJy in 5 ms (1σ).

Observations in August and September were searched by a prototype version of *realfast*[2]. *realfast* is a real-time, fast imaging transient search system. The current prototype runs on CPU-based hardware that is normally dedicated to the VLA correlator; for this experiment, it runs the transient search pipeline software called *rtpipe*[3]. Images were formed for each integration with DMs of 0, 546, 556.9, 560, and 565 pc cm^{-3} and a time resampling grid of 5, 10, 20, 40, and 80 ms. This DM grid was chosen to maintain 90% sensitivity to the nominal DM range of 540–570 pc cm^{-3}. Gain calibration was made from observations of J0555+3948 by an automated system (telcal), which uses phase-only calibration. A flux scale was calculated for each spectral window from an observation of 3C48 and applied to all burst spectra and has an accuracy of about 10%.

Burst detections and localizations were made within 5–10 hours of data being recorded. The transient search starts when data are recorded and proceeds slower than real-time, so we refer to it as "quasi real-time". For each trial DM, integration, and time scale, we form an image and calculate the S/N ratio for the peak pixel in the dirty image. We empirically identified S/N thresholds

[2] See `http://realfast.io` and (Law et al. 2017).

[3] See `https://github.com/caseyjlaw/rtpipe` and Law et al. (2015).

of 6.4 and 7.4 as useful to capture data quality statistics and candidates for inspection, respectively. The higher threshold is relatively unlikely to be triggered by thermal noise in this configuration, so *realfast* generates a more detailed (and computationally intensive) candidate visualization that includes an image and spectrum. All visibilities are recorded so detailed analysis, including improved calibration and localization, can be conducted offline.

2.2. *Arecibo*

Arecibo observed with the L-wide receiver using the PUPPI pulsar backend. The observational frequency range was 1.15 to 1.73 GHz and frequency resolution was 1.5625 MHz, which has a typical sensitivity of 2 mJy in 2 ms (1σ). We recorded total full Stokes polarization intensity spectra with a time resolution of 10.24 μs. Each frequency channel was coherently dedispersed to 557 pc cm^{-3}, significantly reducing intra-channel dispersion smearing. The full width at half maximum (FWHM) beam size at band center is $3.3'$.

In total, 11 Arecibo observations had some simultaneous coverage with the VLA. All of these observations were conducted after the VLA localization, so they were pointing directly at FRB 121102. Three of those observations had simultaneous coverage of VLA bursts and one of those Arecibo observations detected the VLA burst. Overall, there were many more bursts detected at Arecibo than with the VLA, including some Arecibo bursts with simultaneous VLA upper limits. A more detailed analysis of those bursts will be presented elsewhere (Michilli et al, in prep).

2.3. *Effelsberg*

Effelsberg observations were conducted with the S60mm receiver and recorded total intensity spectra with the PFFTS backend in pulsar search mode. The observations had a time resolution of 65.5 μs and 128 frequency channels. The receiver has a system equivalent flux density of 18 Jy and a FWHM beam size of $2.4'$ at 4.85 GHz.

Five Effelsberg observations were made pointing at the known location of FRB 121102 and had some simultaneous coverage with the VLA. Two of these observations were simultaneous with VLA bursts. The nominal receiver bandwidth is from 4.6 to 5.1 GHz, but a configuration error reduced effective bandwidth to 100 MHz centered at 4.85 GHz for both of these observations during VLA bursts. The sensitivity in these observations was about 28 mJy in 2 ms (1σ), which is two times worse than the full-bandwidth value. No burst was detected in either observation.

2.4. *LWA1*

Beginning in April 2016, VLA observations of FRB 121102 were simultaneously observed with LWA1 when possible. The LWA1 observations were automatically scheduled through the Heuristic Automation for LWA1 (HAL) system. Briefly, the HAL system receives messages via the internet that signal the start of a VLA observation. If the source is visible and there are no high priority LWA1 observations scheduled, the HAL system automatically generates an observing schedule, re-configures the telescope, and alerts the observatory staff of the change. The time delay from HAL receiving a message to starting an observation is typically one to two minutes.

The LWA1 observations consisted of single phased-array beam centered on the location of FRB 121102 with two 4096-channel spectral windows spanning frequencies from 52.2–71.8 MHz and 68.2–87.8 MHz. The observations were taken in a spectrometer mode with a channel size of 4.8 kHz and a sample time of 160 ms. The integration time was set to be equal to the dispersion smearing across a single channel at 50 MHz for DM$\approx$ 560 pc cm^{-3}.

Two of the VLA detected pulses, on MJD 57648 and 57649, had simultaneous coverage with LWA1. We use the modeled LWA1 antenna sensitivity as a function of zenith angle to estimate an system equivalent flux density of 9.5 kJy and 8.7 kJy for the two bursts, respectively. The data were de-dispersed into time series with DMs ranging from 500 to 600 pc cm^{-3} using a step size of 1.0 pc cm^{-3}. Each spectral window was searched using PRESTO (Ransom 2001) with a boxcar matched-filtering width from the native time resolution up to 48 seconds. We also visually inspected the dedispersed time series for the DM range 557 to 560 pc cm^{-3}.

No dispersed pulses were found with significance greater than 10σ equivalent to a flux density limit of $\sim$ 60 Jy for a width of 160 ms. The system equivalent flux density does not change much between the two windows. The effective sensitivity to a typical 2 ms pulse width is 4.8 kJy.

2.5. *AMI-LA*

We observed FRB 121102 with AMI-LA for 3 hours each on four epochs starting at MJDs 57638, 57643, 57645, 57646, 57648, and 57649. Observations were made with the new digital correlator having 4096 channels across a 5 GHz bandwidth between 13–18 GHz with a 1 s integration time. The phase calibrator, J0518+3306, was observed every 12 minutes for about 1.5 minutes. The AMI-LA data were binned to eight 0.625 GHz channels and processed (interference exci-

sion and calibration) with a fully-automated pipeline, AMI-REDUCE (e.g., Perrott et al. 2013). Daily measurements of 3C48 and 3C286 were used for the absolute flux calibration, which is good to about 10%.

We inspected the calibrated visibilities, and did not find any signal above 30 mJy in the 1 s samples at and in the vicinity of the detected bursts. This corresponds to a sensitivity of 15 Jy for an assumed pulse width of 2 ms. Concatenating and imaging the 12 hours of calibrated data with the CASA tasks *concat* and *clean* also does not yield any significant detection at the FRB location. Although the statistical 3σ upper limit is 60 μJy, extended mJy-level sources in the field cause sidelobe confusion (the AMI-LA angular resolution is $\sim 30''$), and the actual upper limit is larger. We introduced artificial point sources at the FRB location using the CASA *sm* tool, and found that these sources can be recovered at 3σ as long as their peak flux densities are more than $\sim$ 100 μJy. Hence, we place an upper limit of 100 ± 10 μJy on any quiescent or possible radio flaring on $\sim$days timescales from the FRB. This limit is similar to the flux density measured by the VLA at 12 GHz for the persistent source (Chatterjee et al. 2017).

3. RESULTS

3.1. *Multi-Observatory Burst Spectrum*

Figure 2 shows a dynamic spectrum for the first FRB burst to be detected simultaneously at two telescopes. This burst, on MJD 57648, was detected both by the VLA and Arecibo while upper limits were measured by simultaneous observations at the other three telescopes. In total, four of the VLA bursts had simultaneous observing coverage with either Arecibo, Effelsberg, LWA1, or AMI-LA. Two of the VLA bursts had simultaneous observing coverage by all four observatories, including the burst detected by Arecibo (Figure 1).

To generate the multi-telescope dynamic spectrum, the VLA data were resampled to the Arecibo temporal grid after correcting for barycentric and dispersion measure offsets. We assumed a DM of 560.5 pc cm^{-3} (Hessels et al., in prep) to calculate a dispersion delay of 189 and 734 ms from infinite frequency to the top of the VLA and Arecibo bands, respectively. An error in the DM of 1 pc cm^{-3} corresponds to a delay time correction error of 0.3 and 1.4 ms for the VLA and Arecibo bands, respectively. We used PRESTO to calculate a relative barycentric time correction of 3.8 ms between the VLA and Arecibo at the time of observation.

The regridded dynamic spectrum has an apparent DM error that is evident both as a frequency-dependent time drift within the Arecibo observation and as an offset between the Arecibo and VLA bursts. Both of these drifts are consistent with an apparent DM of $\sim$565 pc cm^{-3}. More refined modeling of the VLA dynamic spectrum alone (§3.2.1 and Table 2) are consistent with this higher DM value.

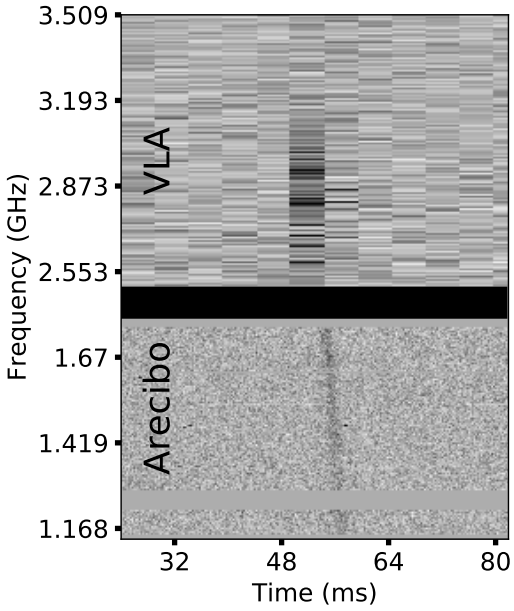

Figure 2. Composite dynamic specrum for the burst from FRB 121102 on MJD 57648 with data from the VLA and Arecibo observatories. The time axis is measured in milliseconds relative to MJD 57648.437788874842 with times corrected to the barycenter and infinite frequency (assuming DM= 560.5 pc $^{-3}$). The thick black line separates data from the VLA (2.5 to 3.5 GHz) and Arecibo (1.1 to 1.8 GHz) and flagged data are grey. For clarity, the VLA and Arecibo data are independently normalized to units of S/N per pixel; Arecibo is 5 times more sensitive than the VLA.

Figure 3 shows coarse spectra built from integrated flux densities measured (or limited) for the three VLA bursts with observing coverage by Arecibo or Effelsberg. The burst on MJD 57648 was detected with VLA and Arecibo with significances of 25σ and 39σ, which corresponds to peak flux densities in 5 ms of 111 ± 5 mJy and 14 ± 0.4 mJy at 3 and 1.4 GHz, respectively. The VLA observations underresolve the pulses in time, so to compare these values, we assume a typical pulse width of 2 ms. Under this assumption, the VLA and Arecibo integrated flux densities are 278 ± 13 and 64 ± 2 mJy at 3 and 1.4 GHz, respectively. Assuming a power law flux density model ($S_\nu \propto \nu^\alpha$), we find a spectral index $\alpha = 1.9$. This is inconsistent with the spectral index limit implied by the Effelsberg nondetection at 4.5 GHz ($\alpha < -1.7$ for a 2 ms burst and 5σ limit).

Overall, the bursts with simultaneous observing coverage are not well described by a power-law model. Two Arecibo nondetections and two Effelsberg nondetections of VLA bursts place mutually inconsistent lower and upper limits on the spectral index. The Arecibo and Effelsberg upper limits at 1.4 and 4.5 GHz, respectively, limit all burst spectral indices $\alpha_{1.4/3} > +4.8$ and $\alpha_{3/4.5} < -2.7$. These are consistent with limits from the LWA1 and AMI-LA, which require $\alpha_{0.07/3} > -2.4$ and $\alpha_{3/15} < 1.5$ for bursts on MJD 57643 and 57649 (the brightest VLA bursts with observing coverage), respectively. The strictest limits on $\alpha_{1.4/3}$ and $\alpha_{3/4.5}$ are both derived from the burst on MJD 57649, which shows that a power law model is inappropriate even for a single burst.

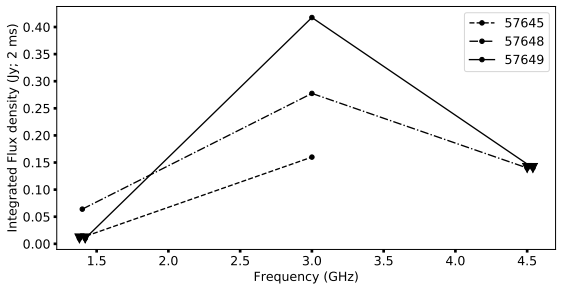

Figure 3. Broadband spectral measurements and limits for three bursts of FRB 121102 with observing coverage by Arecibo or Effelsberg. Upper limits assume a pulse width of 2 ms and a 5σ detection threshold. Measurements (dots) and limits (triangles) are shown for Arecibo, VLA, and Effelsberg at 1.4, 3, and 4.5 GHz, respectively; limits from LWA1 and AMI-LA are not visible on this scale. Errors in flux density are comparable to the symbol size and are not shown. Overlapping points are offset by tens of MHz in frequency for clarity.

3.2. *VLA Bursts*

3.2.1. *Spectrotemporal Modeling*

This paper refines the analysis of the nine VLA radio burst spectra described in Chatterjee et al. (2017) in a few ways. We use a better calibration scheme and have optimized the detection significance over a fine grid of DM (ΔDM = 1 pc cm^{-3}). After calibration and flagging, the visibility phases were rotated to the best-fit location (RA, Dec = 05h31m58.70s, +33d08m52.5s; Chatterjee et al. 2017) to extract a Stokes I spectrum that maximizes the image S/N for each burst.

Table 2 summarizes the spectrotemporal properties of all nine VLA bursts. Parameters such as integrated flux density, S/N, and Stokes V were measured from the burst properties integrated in frequency. Stokes V values were estimated from the dual-circular feeds as $(RR - LL)/(RR + LL) \approx 3\%$, which is comparble to the systematic error expected from beam squint at this location in the primary beam [4]. Given that systematic effects dominate the apparent circular polarization, this observation limits the fractional circular polarization to less than 3%.

Figure 4 shows that the Stokes I spectra are generally characterized by a broad, Gaussian shape with inter-channel modulation as high as 100%. Diffractive scintillation from the Milky Way has a typical bandwidth of 7 MHz along this line of sight (Cordes & Lazio 2002), which is similar to the channel size of 4 MHz. The burst energy is calculated from the flux density in 5 ms and integrating over the optimal Gaussian spectral model.

The dynamic radio spectra (time versus frequency) were modeled using a Markov chain Monte Carlo (MCMC) method. We used the Goodman and Weare affine invariant sampler (Goodman & Weare 2010) as implemented in *emcee* (Foreman-Mackey et al. 2013). The dynamic spectra were modeled prior to dispersion correction. The spectral structure was modeled as a broad Gaussian envelope as a function of channel "ch" as:

$$G(\mathrm{ch}) = \frac{\mathrm{amp}}{\sqrt{2\pi}} \exp\left[-\frac{1}{2}\left(\frac{\mathrm{ch} - \mathrm{center}}{\sigma_{\mathrm{ch}}}\right)^2\right] \qquad (1)$$

where "amp" is in mJy per 5 ms integration, "center" is the Gaussian center channel, and σ_{ch} is its width. The arrival time was modeled with a cold plasma dispersion law with the arrival time in units of integrations of:

$$\mathrm{i(ch)} = \mathrm{i0} + 4.1488\times10^{-3}\,\mathrm{DM}\left[\mathrm{f(ch)}^{-2} - \mathrm{f(ch0)}^{-2}\right]/(5\mathrm{ms}) \qquad (2)$$

where "i0" is the arrival time at the highest frequency, "ch0", and function "f" maps the channel to a frequency in units of GHz. Finally, the pulses were assumed to have an intrinsically square temporal width (parameter W_{int}). This 6-parameter model defined the intrinsic signal that was then distributed over a fixed time-frequency observing grid.

We use a log likelihood function $\ln \mathcal{L} = (-1/2)\sum_i (S_i - S_{i,\mathrm{model}})^2/\sigma_s^2$, where S_i refers to the measured and modeled flux density in a single pixel of the dynamic spectrum and $\sigma_s \approx 70$ μJy is the measured off-burst noise per 5 ms integration and 4 MHz channel. A flat prior was used over all ranges with valid data with the requirement that the integrated signal must have a detection significance higher than 8σ. The 6-dimensional models

[4] See EVLA memo #195 at `https://library.nrao.edu/public/memos/evla/EVLAM_195.pdf`.

Table 2. Properties of FRB 121102 Bursts Seen by VLA at 3 GHz

Time		Observed properties			Modeled properties					
Calendar day (2016)	Burst time (MJD)	S/N (image)	$S_{\rm I,5\ ms}$ (mJy)	$S_{\rm V}$ (mJy)	DM (pc cm^{-3})	W (ms)	$S_{\rm I,peak}$ (mJy)	Center (GHz)	FWHM (MHz)	$E_{\rm int}$ (10^{38} erg)
23 Aug	57623.74402686	38	194	+3	567±2	2.0±0.2	690	2.8	290	12
2 Sep	57633.67986367	179	1500	–35	568.2±0.2	2.05±0.02	3340	3.2	510	98
2 Sep[c]	57633.69515938	15	69	+2	562^{+4}_{-6}	$2.5^{+0.9}_{-0.6}$	>430	<2.5	<290	7
7 Sep	57638.49937435	12	55	+5	567^{+7}_{-9}	$1.3^{+1.4}_{-0.8}$	130	3.1	420	3
12 Sep[a]	57643.45730263	100	508	–5	$565.6^{+0.6}_{-0.5}$	1.9±0.1	1170	2.8	510	34
14 Sep[a]	57645.42958602	13	64	+3	563^{+5}_{-4}	1.1±0.7	170	2.8	380	4
15 Sep[c]	57646.46600650	20	87	+1	569±5	$2.5^{+0.9}_{-1.4}$	>420	<2.5	<430	10
17 Sep[a,b]	57648.43691490	25	111	+9	564±2	$1.4^{+0.3}_{-0.4}$	260	2.8	470	7
18 Sep[a]	57649.45175697	36	167	+1	567±2	2.1±0.5	290	3.0	690	12

NOTE—$S_{\rm V}$ is the measured circular polarization of the burst, which dominated by systematic effects. All error ranges represent 68% confidence intervals.

[a] Simultaneously observed by either Arecibo, Effelsberg, LWA1, or AMI-LA.

[b] Detected simultaneously with Arecibo.

[c] Best-fit Gaussian is not centered in 3 GHz band, so spectral parameters are limits.

were sampled with 100 chains taking 700 steps; we ignored the first 200 steps to properly sample the posterior distributions.

The parameters for the best model of the dynamic spectrum are given in Table 2 and the resulting Gaussian model overlaid on Figure 4. Two of the best-fit Gaussians are centered at the boundary of the 3 GHz band, so parameter estimates are actually limits. The other seven best-fit models appear contained by the 1 GHz wide band (> 90% of the modeled flux is within the 3 GHz band). In all cases, the typical burst spectrum has a FWHM of approximately 500 MHz. This confirms previous reports based on Arecibo and GBT data (Scholz et al. 2016) with the wider (1 GHz) VLA bandwidth and extends this phenomenon to 3 GHz.

Our approach simultaneously models the spectral and temporal evolution of the burst. A typical FRB 121102 burst takes ∼ 180 ms or 36 integrations to cross the observing band from 2.5 to 3.5 GHz. The effect of a finite pulse width is visible as the burst moves from one integration to the next, even for widths narrower than the integration time of 5 ms. Table 2 shows that the typical burst width is measured as 2 ± 0.5 ms (68% confidence interval); the inter-channel dispersion smearing ranges from 0.4 to 1.1 ms across this band. The brightest burst (on MJD 57633.68) is modeled with a temporal width of 2.05 ± 0.02 ms and its arrival time is measured with a precision of ~ 50 μs. Note that these errors are only accurate to the degree that the model represents the data. One potential bias in the model is that we do not model scintillation effects.

While most bursts are modeled with well-defined parameter probability distributions, one burst is an outlier. Figure 5 shows the scatter plot matrix (Foreman-Mackey 2016) for the MCMC run on burst 57646. Two clusters of samples are identified for this burst: one narrow, low-DM and one wide, high-DM. Assuming that the model is appropriate, this implies that the burst can be decomposed into two subbursts.

3.2.2. *Dispersion*

The spectrotemporal modeling presented in §3.2.1 provides marginalized posterior distributions for burst DM and pulse width. Figure 6 compares the 68% confidence intervals on the DM for all nine VLA bursts against detection time (top panel) and the modeled burst temporal width (bottom panel). The error weighted mean burst DM is 567.8±0.1 pc cm^{-3}, significantly larger than the long-term average of 560.5 pc cm^{-3} seen by Arecibo during this campaign. Furthermore, several of the 95% confidence intervals in DM are not consistent with this mean nor each other, which suggests that some burst-specific property can bias the measured DM. The variation in DM observed by the VLA at 3 GHz is similar to that reported for Arecibo observations of FRB 121102 in Scholz et al. (2016).

The bottom panel of Figure 6 compares the DM to the modeled temporal width of the bursts. There is a weak correlation between burst width and apparent DM. A

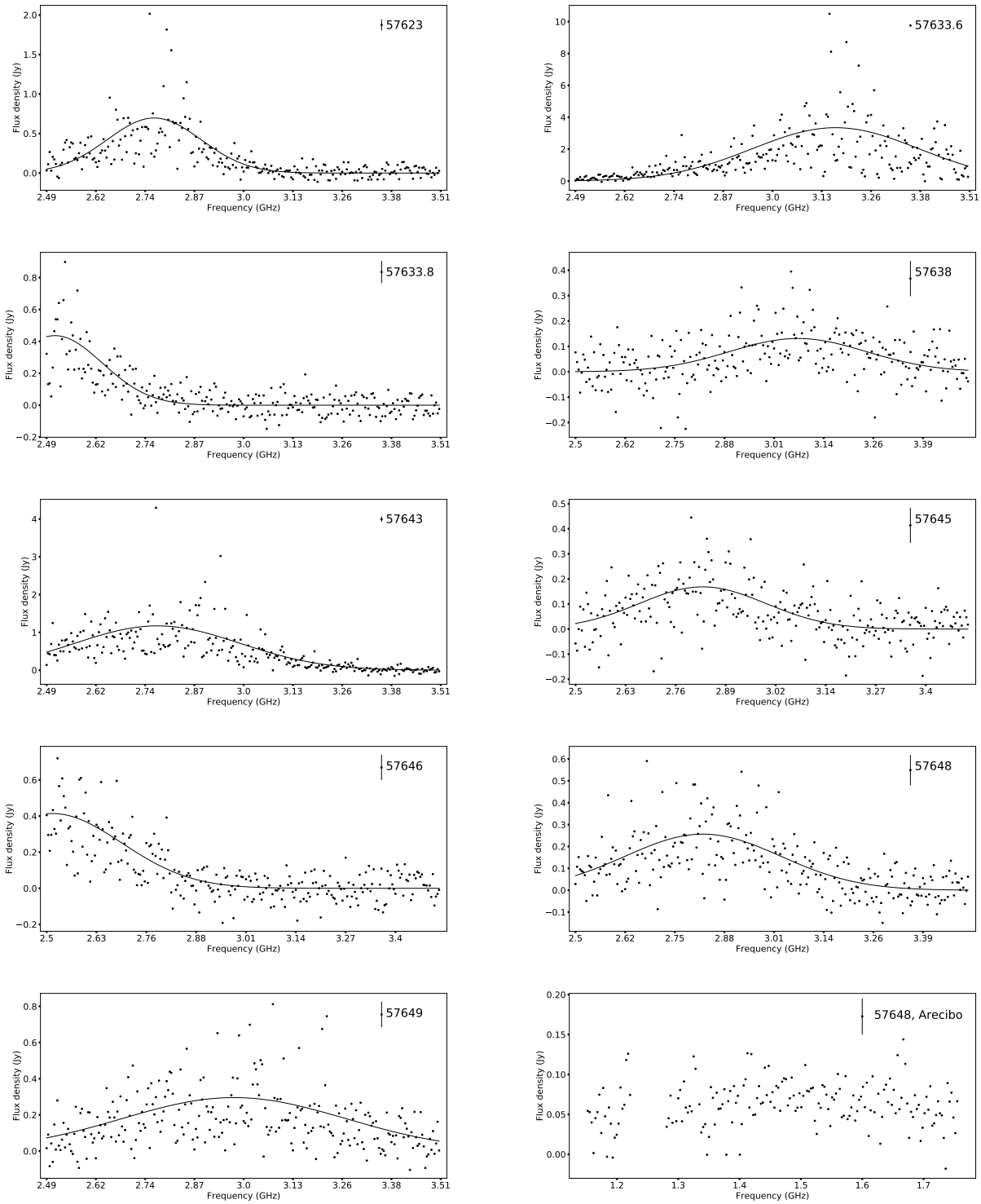

Figure 4. Ten panels show spectra for nine VLA bursts and one Arecibo burst (bottom right). The VLA spectra are drawn from flux-calibrated, dedispersed 5 ms integrations. The Arecibo spectrum is drawn from a 2.7 ms window with 3.125 MHz channels and the flux scale is esimated using the radiometer equation. The solid line shown with VLA spectra is a best-fit Gaussian model found through modeling. The typical VLA flux density error per channel is 70 mJy, which is shown at the top right of each panel next to the MJD label.

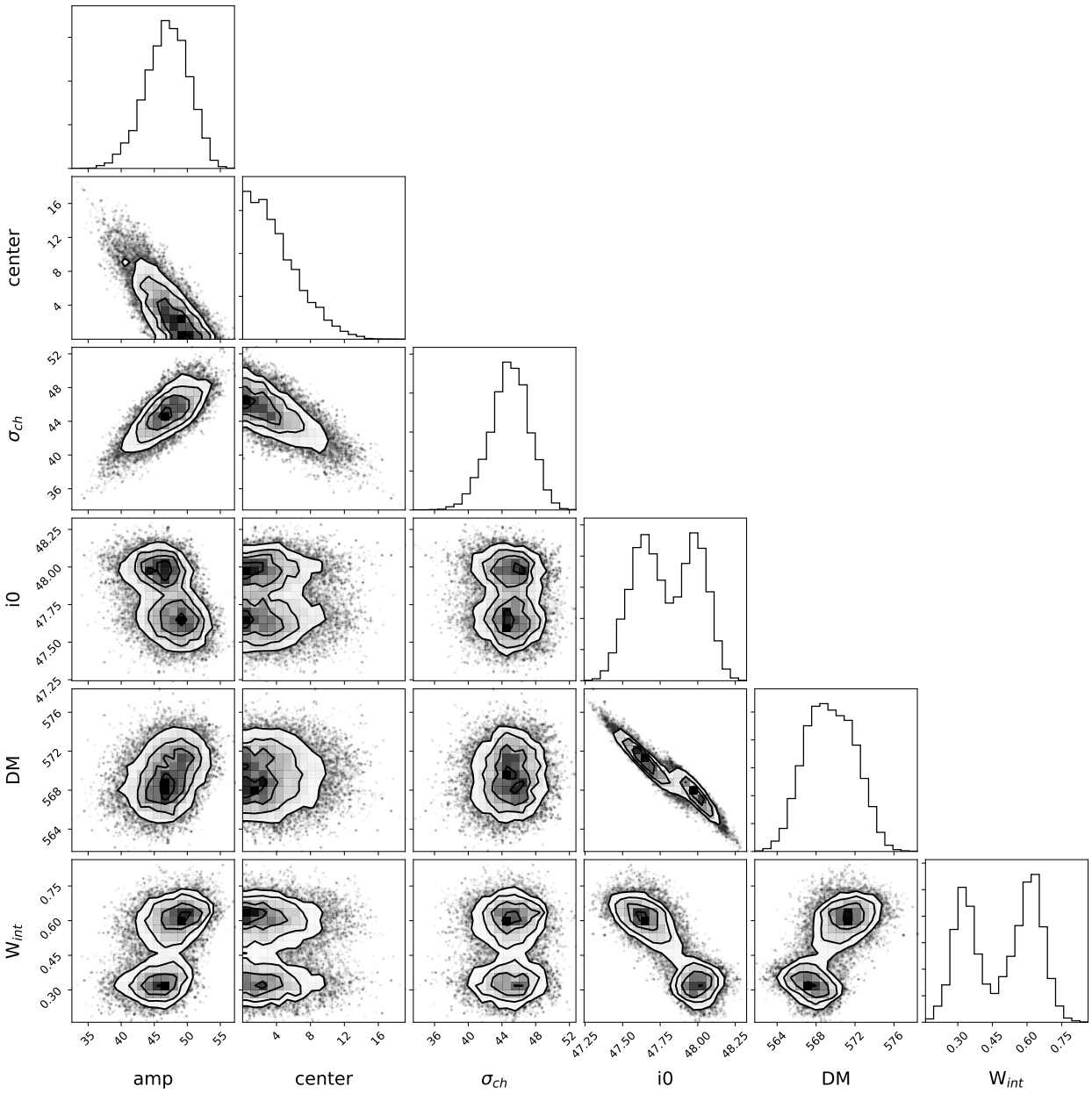

Figure 5. A scatterplot matrix that shows the correlation of every pair of parameters in the MCMC run for burst 57646. The equivalent plot for the other bursts show normally-distributed samples, but this burst shows significant structure in the samples. The parameters "amp", "center", and "σ_{ch}" refer to the Gaussian spectral shape, while "DM", "i0", and "W_{int}" refer to the temporal shape. The parameters are given in units of channels (4 MHz) and integrations (5 ms).

change in width of ~ 1 ms correlates with a change in apparent DM of approximately 5 pc cm^{-3}.

3.2.3. *Fine Spectral Structure*

The spectral fits in Figure 4 have residuals that include single samples that deviate by many standard deviations, particularly in the bursts on MJDs 57623, 57633.6, and 57643. These do not appear to be caused by terrestrial interference. They are most likely spectral variations from diffractive interstellar scintillations that, as noted previously, have characteristic frequency widths slightly larger than the 4 MHz channel bandwidth. Scintillation variations are multiplicative and have a one-sided exponential probability distributino function that can yield occasional large-amplitude "scintles" that are several times the mean scintle amplitude of unity.

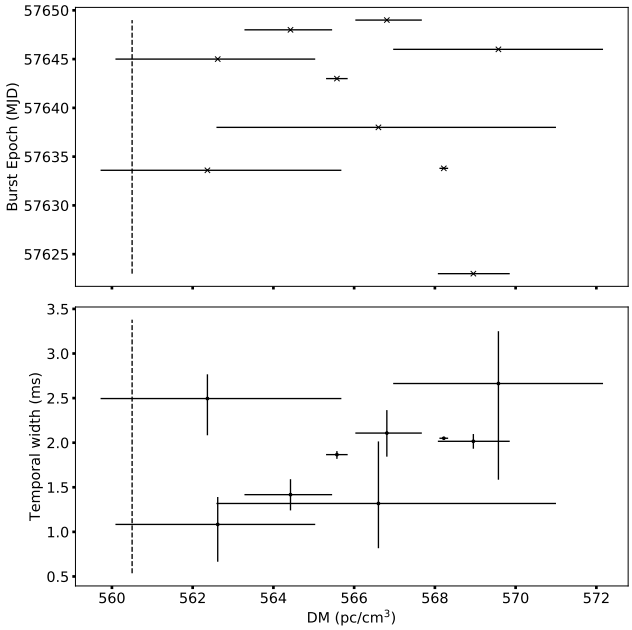

Figure 6. (Top) Burst epoch versus DM for nine 3 GHz bursts detected by the VLA. The DM scale for both panels is shown at the bottom. The 68% confidence interval on DM is shown with a bar and the dashed line shows the best-fit DM= 560.5 pc cm^{-3} inferred from Arecibo observations at 1.4 GHz (Hessels et al, in prep). (Bottom) Temporal width versus burst DM for the same nine VLA bursts.

The spectral variations could in principle also include contributions from self noise in the source but to be significant, intrinsic fine structure in the burst would have to be on microsecond scales.

3.3. *Temporal, Energy, and Brightness Distributions of Bursts*

The burst rate for FRB 121102 varied dramatically throughout the 2016 observing campaign. In the early-2016 campaign, we observed for 30 hours at 3 GHz and no bursts were detected. In the late-2016 observing campaign, we observed for 27 hours at 3 GHz and detected nine bursts. Overall, the data quality is uniform and high, so the inhomogeneous burst distribution shows that the burst rate was not uniform.

Assuming that the burst detection probability follows a Poisson distribution, the mean VLA, 3 GHz burst rate is $R = 0.16 \pm 0.05$ hr^{-1} above a fluence of 0.2 Jy ms. The nondetection in the first half of 3 GHz observing limits the FRB rate to $R < 0.1$ hour^{-1} (95% confidence limit). The 3 GHz burst rate was much higher during the late-2016 campaign, $R = 0.3 \pm 0.1$ hour^{-1}.

The integrated burst flux density is calculated by integrating the burst spectral model (Table 2) in frequency and time. Some VLA burst spectra seem to be contained by the 2.5 to 3.5 GHz band and most of them seem to have Gaussian envelopes that are well modeled by the emission within that band. Assuming that the Gaussian shape defines the full emission window, the integrated 3 GHz flux density can be converted to a total energy with no further assumptions about the burst spectral properties as:

$$E_{\rm int} = ({\rm amp\ 5\ ms})(\sigma_{\rm ch}\ 2.3554\ {\rm MHz})10^{-23}(4\pi {\rm L}_{\rm d}^2)\ {\rm erg} \quad (3)$$

where the first term represents the burst fluence, the second term represents the integral of the burst spectrum, and L_d is the luminosity distance to the source.

Figure 7 shows the FRB 121102 burst energy cumulative distribution as seen by the VLA and calculated from prior observations by Arecibo and the Green Bank Telescope (Spitler et al. 2016; Scholz et al. 2016). The latter two energy distributions are scaled from the fluence by assuming that all burst energy is included by the observation. This likely underestimates the burst energy for some bursts, but should not affect the slope of the distribution. The VLA distribution represents a relatively long campaign, so it is sensitive to lower event rates, but is less sensitive than the single-dish campaigns shown (minimum $E_{\rm int} \approx 3 \times 10^{38}$ erg). We also show the rate upper limit (95% confidence) from the early-2016 VLA campaign to demonstrate that even identical observing campaigns have different detection rates.

We modeled the differential energy distribution, $dN/d\log E$, again using a Poisson detection probability with a rate function $\lambda = AE^{\alpha}$. Rather than trying to estimate a completeness limit for each energy distribution, we assume an effective detection limit of 0.9 times the weakest burst detected; the best-fit slope is weakly dependent on this, but general conclusions are robust. We directly sampled the likelihood distribution to estimate a best slope of $\alpha_{\rm VLA} = -0.6^{+0.2}_{-0.3}$, $\alpha_{\rm Arecibo} = -0.8^{+0.3}_{-0.5}$, and $\alpha_{\rm GBT} = -0.8^{+0.4}_{-0.5}$ (68% confidence interval). Expressed as a power law function in dN/dE, the slope index is approximately –1.7. We caution that propagation effects can potentially modulate the intrinsic flux density and significantly affect any interpretation about burst amplitudes.

4. DISCUSSION

4.1. *Burst Spectra*

We present the first simultaneous detection of an FRB with multiple telescopes and over frequencies from 1.2 to 3.5 GHz. The flux density of the Arecibo burst detected on MJD 57648 is an order of magntude less than that seen by the VLA. At the same time, three other bursts from FRB 121102 had similar observing coverage but were not detected simultaneously. This is consistent

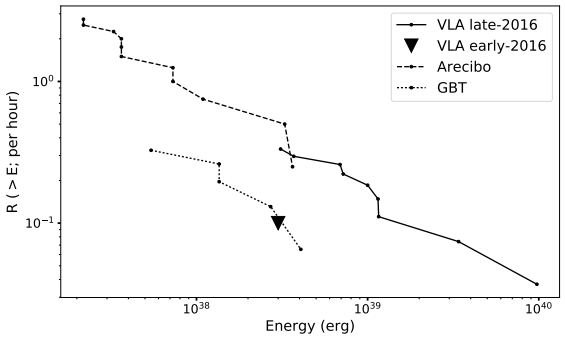

Figure 7. The cumulative burst energy distributions for the VLA, Arecibo, and GBT bursts are shown with dots connected by solid, dashed, and dotted lines, respectively. The Arecibo distribution is derived from the 11 1.4 GHz bursts reported in Spitler et al. (2016) and the GBT distribution is derived from the 5 1.4 GHz bursts reported in Scholz et al. (2016). An upper limit from the VLA nondetection in early 2016 is shown as a triangle.

with the spectral structure observed within the 3 GHz VLA band, which is typically limited to a Gaussian envelope with width of roughly 500 MHz. This confirms earlier results at 1.4 GHz (Spitler et al. 2016; Scholz et al. 2016) with a wider bandwidth and extends the presence of this phenomenon to 3 GHz.

If FRB 121102 burst spectra are typical of the larger FRB population, then population models need to be generalized beyond the assumption of a spectral power law. Most obviously, FRB 121102 implies that future multi-telescope searches for bursts are unlikely to simultaneously detect bursts in different bands (c.f. Sallmen et al. 1999). Second, since burst spectra have limited bands, the burst detection rate at one frequency may not represent that at another. Rate estimates for the FRB population will need to explicitly account for the frequency-dependent rate. Finally, we note that the odds of detecting a burst will improve with bandwidth beyond the gain in sensitivity, since bandwidths wider than the FRB characteristic width are more likley to cover the burst envelope. However, FRB search algorithms will need to be modified to search for bursts with spectral width less than the full bandwidth.

After correcting for barycentric and typical dispersion delays, the burst spectra at the VLA and at Arecibo show a residual temporal drift. This drift can be interpreted as an excess DM, but contemporaneous observations at 1.4 GHz measured a significantly lower DM (560.5 pc cm^{-3}; Hessels et al, in prep). This excess DM is comparable to the burst-to-burst variation in DM within the whole sample of VLA 3 GHz bursts. This variation had been noted in earlier 1.4 GHz Arecibo observations of FRB 121102 (Scholz et al. 2016), but the VLA bursts demonstrate that this burst-specific DM is seen simltaneously from 1.4 to 3 GHz.

One interpretation for the burst-dependent DM is that the bursts have a frequency-dependent pulse shape. Pulsar pulse shapes evolve with frequency on GHz frequency scales, presumably due to changes in the beam shape (Lyne & Manchester 1988). The burst-dependent DM changes are on the order of 1% of the total DM (equivalent to a delay rate up to 2 ms GHz^{-1}), which is much larger than typically observed (Lentati et al. 2017). Our modeling of the VLA burst dynamic spectra show a weak correlation between larger apparent DM and pulse width. This could be a signature of unresolved spectrotemporal structure in the VLA burst spectra that biases the measured DM.

The burst-specific DM structure could be intrinsic to the emission mechanism or induced during propagation. Radio waves can be modified in a variety of ways (e.g., scintillation, scattering) and the duration of the emission in the source frame is not known (Cordes et al. 2016). Cordes et al. (2017) describe a model where plasma lensing near the source of an FRB can magnify radio emission by orders of magnitude. Plasma lensing can also produce multiple burst images separated by time scales from microseconds to tens of milliseconds or longer. These burst images would also have slightly different DMs. Lensing amplifications have a complicated frequency dependence that includes spikes, plateaus, and troughs. The simultaneous detection of burst MJD 57648 with both Arecibo (L band) and the VLA (S band up to 3.2 GHz) suggests requires a focal frequency $\gtrsim 3.2$ GHz and sufficient amplification in both bands.

4.2. *Energy Distribution*

Our refined analysis shows that FRB 121102 has even higher isotropic energies than previously reported for FRB 121102, reaching energies $E_{\rm max} \approx 10^{40}$ erg. While this emission is coherent and beamed, the apparent energy is larger than Galactic analogues such as the giant pulses from the Crab pulsar ($\sim 10^{35}$ erg, $T_{b,\rm Crab} \sim 10^{41}$ K; Hankins et al. 2003; Katz 2014). Radio bursts from FRB 121102 require either dramatic scaling of known emission processes (Lyutikov et al. 2016; Cordes & Wasserman 2016) or strong amplification by propagation effects (Cordes et al. 2017).

In §3.3 we compare the energy distribution of the 9 VLA bursts to those reported earlier by Arecibo and the GBT. All three energy distributions can be characterized as a power law in dN/dE with slope ~ -1.7.

This slope is seen even though the burst rate varies by almost an order of magnitude between observations and frequencies cover both 1.4 and 3 GHz bands. This suggests that the slope is related to the underlying physical process, rather than the burst detection rate at any given time. The value of the energy distribution slope is similar to that derived from high-energy bursts from magnetars (Göğüş et al. 2000; Scholz & Kaspi 2011), which may be examples of self-regulated critical phenomena (slope= $-5/3$; Aschwanden 2011). This is consistent with the idea that magnetar bursts can generate both the millisecond-duration bursts and persistent radio emission from FRB 121102 (Beloborodov 2017).

4.3. *Flux Distribution*

New FRB discoveries have often surprised observers with their remarkable brightness (Lorimer et al. 2007; Ravi et al. 2016). When modeling the flux distribution as a power law, an isotropic distribution of sources will have a power law index, α, of –1.5. Prior to the measurement of the first GRB redshift, deviations from this Euclidean distribution were used to infer their cosmological distribution (e.g., the $V/V_{\rm max}$ test; Mao & Paczynski 1992; Fenimore & Bloom 1995). Multiple studies have suggested that FRBs have a sub-Euclidean flux distribution ($-0.5 < \alpha < -0.9$; Vedantham et al. 2016; Li et al. 2016; Lawrence et al. 2016). Others have noted that the flux distribution is not well modeled as a power law, such that α is effectively sensitivity (and telescope) dependent (Oppermann et al. 2016; CHIME Scientific Collaboration et al. 2017).

We now know that FRB 121102 would be detectable with the VLA out to $z = 0.7$, which suggests that cosmological effects are even more important for understanding properites of the FRB population. CHIME Scientific Collaboration et al. (2017) demonstrate how redshift space distortions, time dilation, and spectral index ("k-correction") effects can flatten the flux distribution. To this complex scene, we add the fact that FRB 121102 burst spectra are not defined by a spectral index, which suggests that k-corrections are likely to be very difficult to calculate in practice. If the FRB burst rate is higher at low (rest) radio frequencies, then high-redshift FRBs will have an lower (redshifted) rate that flattens the dN/dF distribution in a manner similar to a k-correction. However, propagation effects are expected to suppress the FRB rate at sub-GHz frequencies (Rajwade & Lorimer 2017; Chawla et al. 2017) as well. The VLA and Arecibo observed intensively in a coordinated fashion during the late-2016 campaign and a comparison of their relative rates will be presented elsewhere.

4.4. *Repetition*

The chance of detecting a burst from FRB 121102 with the VLA changes substantially on day–month timescales. A major outstanding question is whether this time-variable rate is driven by an intrinsic process (Katz 2016) or extrinsic (propagation) effects in the host galaxy or intergalactic medium (Cordes et al. 2017). However, the temporal distribution of VLA detections alone shows that the FRB 121102 burst rate is significantly correlated on short timescales. That is, detecting a burst predicts that you are more likely to find another burst soon thereafter and not detecting a burst predicts you will likely not detect another burst soon thereafter.

The clustering of burst times for the whole FRB population has been modeled as a "red spectrum" (Connor et al. 2016a), while recent work has modeled FRB 121102 burst times with a modified Poisson distribution (Oppermann & Pen 2017). Both temporal models imply that existing observational constraints on repetition are weaker than expected from Poissonian statistics (Petroff et al. 2015; Law et al. 2015). If the clustered bursts are typical of the FRB population, then wide, shallow surveys are the preferred strategy for blind detection of FRBs. Also, since "bursts predict bursts", many short observations are more likely to detect an FRB than a single long observation of the same total length and all new FRB detections should be immediately and intensively followed up.

4.5. *Volumetric Rate of FRB Sources*

Thornton et al. (2013) estimated an isotropic rate of FRB events of 10^{-3} galaxy^{-1} yr^{-1} by calculating the number of Milky Way-type galaxies out to a distance implied by assming all extragalactic DM originates in the IGM ($z \approx 0.9$ for DM$\approx z \times 900$ pc cm^{-3}; Ioka 2003; Inoue 2004). This rate is high (comparable to the rate of core-collapse supernovae; Diehl et al. 2006), which has been used to argue that FRBs are likely not associated with other classes of transient, such as LGRBs or rare subclasses of SNe (Woosley & Bloom 2006). However, since this rate depends on telescope sensitivity, it is not appropriate to compare to other estimates based on source counts.

Here, we reevaluate the FRB volumetric rate by assuming FRB 121102 is a prototype of the class and recasting it as a volumetric rate of FRB sources (i.e., a birth rate). Crudely, the volumetric rate of FRB sources can be defined as $R_{\rm FRB} = R_p/(N_r \Omega_b V(z))$, where R_p is the projected FRB rate, N_r is the number of bursts per source in a typical lifetime, Ω_b is the beaming fraction, and $V(z)$ is the comoving volume out to redshift

z. The newest estimates of the projected FRB rate are 2×10^3 sky^{-1}day^{-1} at high Galactic latitudes and flux densities brighter than 1 Jy ms (Lawrence et al. 2016; Champion et al. 2016; Rane et al. 2016). There is relatively little constraint on the beaming factor, but Galactic pulsars have beaming solid angle fractions on the order of 10% (Tauris & Manchester 1998).

FRB 121102 has an absolute energy scale that can be used to estimate a horizon scale for the typical FRB survey sensitivity. At the typical Parkes survey parameters (e.g., Champion et al. 2016), a survey with a fluence limit of 1 Jy ms can detect FRB 121102 at $z \approx 1$. The distance inferred from the largest DMs observed (~ 1500 pc cm^{-3}; Champion et al. 2016) is somewhat higher, but that likely overestimates distance since DM is expected to have significant contributions from the host galaxy and intervening galaxies (Tendulkar et al. 2017; McQuinn 2014).

Using an assumed horizon redshift of 1, we estimate a rate of $R_{\rm FRB} \approx 5 \times 10^{-5} N_r^{-1} (0.1/\Omega_b)$ Mpc^{-3} yr^{-1}. This calculation ignores time dilation, which underestimates the burst rate by a factor of 2 at the redshift horizon. The narrow burst spectral structure seen for FRB 121102 also suggests that the FRB rate is understated by a factor of a few by ignoring bursts that fall outside the observing band. Finally, we note that this estimate assumes that Galactic latitude and propagation effects do not significantly affect the detectability of FRBs, although scintillation and scattering likely play significant roles (Macquart & Johnston 2015; Cordes et al. 2017).

Despite its many assumptions, this volumetric rate is more appropriate for comparison to rates used for other classes of transient. The LGRB and SLSN-I rates are 10^{-7} and 10^{-8} Mpc^{-3} yr^{-1}, respectively (Guetta & Della Valle 2007; Gal-Yam 2012). Comparing the FRB rate to these rates implies that FRB-emitting sources can be generated in LGRBs and SLSN-I if FRBs repeat 5×10^2 and 5×10^3 times[5], respectively (assuming burst energies of $\sim 10^{40}$ erg). Metzger et al. (2017) use the young magnetar model for FRBs to calculate the maximum number of bursts that can be powered its magnetic field as ≈ 300. Assuming this model for FRBs, LGRBs, and SLSN-I, the rate comparison suggest that the LGRB rate is most consistent with the FRB rate, although there is significant room for adjustment in the models and rate estimate.

5. CONCLUSIONS

The recent precision localization of FRB 121102 has helped identify a host galaxy, measure its distance, and establish it as a member of a truly new class of astrophysical source. With its cosmological distance firmly established, FRB 121102 now serves as a new kind of standard by which FRBs are defined. That fact, combined with a rich data set of many bursts, allows us to apply this source to more general questions about the FRB population.

We presented the first multi-telescope detection (Arecibo and VLA) of an FRB. By detecting this burst from 1.2 to 3.5 GHz, we have demonstrated that some bursts have broad spectral structure. However, the energy of that burst was dominated by the VLA 3 GHz observing band and three other VLA bursts are undetected by simultaneous observations at other telescopes. This demonstrates the burst spectra are poorly described by a power law with a single spectral index. We also modelled dynamic spectra within the VLA 3 GHz band and show that most bursts can be characterized by a Gaussian envelope of width ~ 500 MHz. This modeling also shows that the apparent DM changes from burst to burst and that DM is biased above the long-term average measured at 1.4 GHz. The nature of this DM change is not known, but could be explained by strong frequency-dependent profile evolution or unresolved spectrotemporal structure in the bursts.

With a characteristic burst spectrum, we can estimate total (apparent) radio energy per burst. The cumulative energy distribution is characterized by a power law in dN/dE with slope of ~ -1.7. The amplitude of this power law changes significantly between observational campaigns. The stochastic nature of the burst rate suggests that past constraints on FRB repetition are weaker than previously inferred. The relatively narrow spectral structure, flat energy distribution, and variable burst rate of FRB 121102 suggests that repeated observations, wide bandwidth, and large instantaneous field of view all improve the odds of FRB discovery.

Assuming that FRB 121102 is representative of the FRB population, we calculate a volumetric birth rate of FRB sources that does not depend on telescope sensitivity. We estimate a volumetric rate of FRB sources of $R_{\rm FRB} \approx 5 \times 10^{-5} (0.1/\Omega_b)$ Mpc^{-3} yr^{-1}, which is appropriate for FRB 121102-like burst energies of 10^{40} erg that are detectable out to $z = 1$. This rate is broadly consistent with models of FRBs from young pulsars or magnetars born in superluminous supernovae or long gamma-ray bursts, if the typical FRB repeats on the order of 10^3 times over its lifetime.

New, arcsecond-scale localizations will be critical to refining the picture presented here and constraining

[5] Nicholl et al. (2017) provide a similar estimate of FRB birth rate and reach a similar conclusion.

models of FRB origin. FRB 121102 was localized within hours by a prototype version of *realfast* and an expanded *realfast* system is now under construction. This platform will search a TB/hour data stream in real time in parallel with ongoing VLA observations, potentially detecting and localizing multiple FRBs per year.

ACKNOWLEDGEMENTS

The National Radio Astronomy Observatory is a facility of the National Science Foundation operated under cooperative agreement by Associated Universities, Inc.. Part of this research was carried out at the Jet Propulsion Laboratory, California Institute of Technology, under a contract with the National Aeronautics and Space Administration. This research made use of Astropy, a community-developed core Python package for Astronomy (Astropy Collaboration, 2013). CJL is supported by the University of California Office of the President under Lab Fees Research Program Award 237863 and NSF award 1611606. MAM is supported by NSF award 1458952. KPM's research is supported by the Oxford Centre for Astrophysical Surveys which is funded through the Hintze Family Charitable Foundation. AS gratefully acknowledges support from the European Research Council under grant ERC-2012- StG-307215 LODESTONE. The AMI-LA telescope gratefully acknowledges support from the European Research Council under grant ERC-2012- StG-307215 LODESTONE, the UK Science and Technology Facilities Council (STFC) and the University of Cambridge. PS holds a Covington Fellowship at DRAO. The LWA1 station is supported by the National Science Foundation under grant 1139974 of the University Radio Observatory program. VMK acknowledges support from NSERC, CIFAR, the Canada Research Chair Program and from the Lorne Trottier Chair in Astrophysics & Cosmology.

We thank the VLA staff for their support of *realfast* development and Liam Connor for useful feedback. We acknowledge partial support from the Research Corporation for Scientific Advancement (RCSA) for participation in the meeting Fast Radio Bursts: New Probes of Fundamental Physics and Cosmology at the Aspen Center for Physics (February 12-17, 2017).

Software: *rtpipe*, *realfast*, pwkit (**?**)

REFERENCES

Aschwanden, M. J. 2011, SoPh, 274, 99

Beloborodov, A. M. 2017, ArXiv e-prints, arXiv:1702.08644 [astro-ph.HE]

Champion, D. J., Petroff, E., Kramer, M., et al. 2016, MNRAS, 460, L30

Chatterjee, S., Law, C. J., Wharton, R. S., et al. 2017, Nature, 541, 58

Chawla, P., Kaspi, V. M., Josephy, A., et al. 2017, ArXiv e-prints, arXiv:1701.07457 [astro-ph.HE]

CHIME Scientific Collaboration, Amiri, M., Bandura, K., et al. 2017, ArXiv e-prints, arXiv:1702.08040 [astro-ph.HE]

Connor, L., Pen, U.-L., & Oppermann, N. 2016a, MNRAS, 458, L89

Connor, L., Sievers, J., & Pen, U.-L. 2016b, MNRAS, 458, L19

Cordes, J. M., & Lazio, T. J. W. 2002, ArXiv Astrophysics e-prints, arXiv:astro-ph/0207156

Cordes, J. M., & Wasserman, I. 2016, MNRAS, 457, 232

Cordes, J. M., Wasserman, I., Hessels, J. W. T., et al. 2017, ArXiv e-prints, arXiv:1703.06580 [astro-ph.HE]

Cordes, J. M., Wharton, R. S., Spitler, L. G., Chatterjee, S., & Wasserman, I. 2016, ArXiv e-prints, arXiv:1605.05890 [astro-ph.HE]

Cordes, J. M., Freire, P. C. C., Lorimer, D. R., et al. 2006, ApJ, 637, 446

Diehl, R., Halloin, H., Kretschmer, K., et al. 2006, Nature, 439, 45

Dokuchaev, V. I., & Eroshenko, Y. N. 2017, ArXiv e-prints, 1701.02492, arXiv:1701.02492 [astro-ph.HE]

Ellingson, S. W., Taylor, G. B., Craig, J., et al. 2013, IEEE Transactions on Antennas and Propagation, 61, 2540

Fenimore, E. E., & Bloom, J. S. 1995, ApJ, 453, 25

Foreman-Mackey, D. 2016, The Journal of Open Source Software, 24

Foreman-Mackey, D., Hogg, D. W., Lang, D., & Goodman, J. 2013, PASP, 125, 306

Fuller, J., & Ott, C. D. 2015, MNRAS, 450, L71

Gal-Yam, A. 2012, Science, 337, 927

Goodman, J., & Weare, J. 2010, Communications in applied mathematics and computational science, 5, 65

Göğüş, E., Woods, P. M., Kouveliotou, C., et al. 2000, ApJL, 532, L121

Guetta, D., & Della Valle, M. 2007, ApJL, 657, L73

Hankins, T. H., Kern, J. S., Weatherall, J. C., & Eilek, J. A. 2003, Nature, 422, 141

Inoue, S. 2004, MNRAS, 348, 999

Ioka, K. 2003, ApJL, 598, L79

Kashiyama, K., & Murase, K. 2017, ArXiv e-prints, 1701.04815, arXiv:1701.04815 [astro-ph.HE]

Katz, J. I. 2014, PhRvD, 89, 103009

—. 2016, ApJ, 826, 226
Kulkarni, S. R., Ofek, E. O., Neill, J. D., Zheng, Z., & Juric, M. 2014, ApJ, 797, 70
Law, C. J., Bower, G. C., Burke-Spolaor, S., et al. 2017, in American Astronomical Society Meeting Abstracts, Vol. 229, American Astronomical Society Meeting Abstracts, 330.02
Law, C. J., Bower, G. C., Burke-Spolaor, S., et al. 2015, ApJ, 807, 16
Lawrence, E., Vander Wiel, S., Law, C. J., Burke Spolaor, S., & Bower, G. C. 2016, ArXiv e-prints, arXiv:1611.00458 [astro-ph.HE]
Lentati, L., Kerr, M., Dai, S., et al. 2017, MNRAS, 466, 3706
Li, L., Huang, Y., Zhang, Z., Li, D., & Li, B. 2016, ArXiv e-prints, arXiv:1602.06099 [astro-ph.HE]
Lorimer, D. R., Bailes, M., McLaughlin, M. A., Narkevic, D. J., & Crawford, F. 2007, Science, 318, 777
Lunnan, R., Chornock, R., Berger, E., et al. 2014, ApJ, 787, 138
Lyne, A. G., & Manchester, R. N. 1988, MNRAS, 234, 477
Lyutikov, M., Burzawa, L., & Popov, S. B. 2016, MNRAS, 462, 941
Macquart, J.-P., & Johnston, S. 2015, MNRAS, 451, 3278
Mao, S., & Paczynski, B. 1992, ApJL, 388, L45
Marcote, B., Paragi, Z., Hessels, J. W. T., et al. 2017, ApJL, 834, L8
McQuinn, M. 2014, ApJL, 780, L33
Metzger, B. D., Berger, E., & Margalit, B. 2017, ArXiv e-prints,1701.02370, arXiv:1701.02370 [astro-ph.HE]
Modjaz, M., Kewley, L., Kirshner, R. P., et al. 2008, AJ, 135, 1136
Nicholl, M., Williams, P. K. G., Berger, E., et al. 2017, ArXiv e-prints, arXiv:1704.00022 [astro-ph.HE]
Oppermann, N., Connor, L. D., & Pen, U.-L. 2016, MNRAS, 461, 984
Oppermann, N., & Pen, U.-L. 2017, arXiv:1705.04881
Perrott, Y. C., Scaife, A. M. M., Green, D. A., et al. 2013, MNRAS, 429, 3330
Petroff, E., Johnston, S., Keane, E. F., et al. 2015, MNRAS, 454, 457
Planck Collaboration, Ade, P. A. R., Aghanim, N., et al. 2016, A&A, 594, A13
Popov, S. B., & Pshirkov, M. S. 2016, MNRAS, 462, L16
Rajwade, K. M., & Lorimer, D. R. 2017, MNRAS, 465, 2286
Rane, A., Lorimer, D. R., Bates, S. D., et al. 2016, MNRAS, 455, 2207
Ransom, S. M. 2001, PhD thesis, Harvard University
Ravi, V., Shannon, R. M., Bailes, M., et al. 2016, ArXiv e-prints, arXiv:1611.05758 [astro-ph.HE]
Sallmen, S., Backer, D. C., Hankins, T. H., Moffett, D., & Lundgren, S. 1999, ApJ, 517, 460
Scholz, P., & Kaspi, V. M. 2011, ApJ, 739, 94
Scholz, P., Spitler, L. G., Hessels, J. W. T., et al. 2016, ArXiv e-prints, arXiv:1603.08880 [astro-ph.HE]
Spitler, L. G., Cordes, J. M., Hessels, J. W. T., et al. 2014, ApJ, 790, 101
Spitler, L. G., Scholz, P., Hessels, J. W. T., et al. 2016, Nature, 531, 202
Tauris, T. M., & Manchester, R. N. 1998, MNRAS, 298, 625
Tendulkar, S. P., Bassa, C. G., Cordes, J. M., et al. 2017, ApJL, 834, L7
Thompson, C. 2017, ArXiv e-prints, arXiv:1703.00393 [astro-ph.HE]
Thornton, D., Stappers, B., Bailes, M., et al. 2013, Science, 341, 53
Vedantham, H. K., Ravi, V., Hallinan, G., & Shannon, R. M. 2016, ApJ, 830, 75
Woosley, S. E., & Bloom, J. S. 2006, ARA&A, 44, 507
Zhang, B. 2017, ArXiv e-prints, 1701.04094, arXiv:1701.04094 [astro-ph.HE]
Zwart, J. T. L., Barker, R. W., Biddulph, P., et al. 2008, MNRAS, 391, 1545